Momentum space oscillation properties of vortex states collision

Pengcheng Zhao*

School of Physics and Astronomy, Sun Yat-sen University, 519082 Zhuhai, China

(Received 4 December 2023; accepted 10 April 2024; published 13 May 2024)

A qualitative calculation and discussion of two-vortex-state collisions are given in the scalar ϕ^4 model. Three kinds of vortex states—Bessel, general monochromatic, and Laguerre-Gaussian—are considered. It is found that the total final-momentum distribution in the collision of physical vortex states displays general topological structures, which depend on the initial vortex states' topological charges, which are proportional to the orbital angular momenta. This peculiar matching provides a novel observable, the topological number of momentum distribution, and it may represent a new fascinating research direction in particle physics. We also find that the situation when the angular momenta of the two colliding Laguerre-Gaussian states combine to zero can be recognized by the total final-momentum distribution close to the collision axis. Both features can be used to measure the orbital angular momentum of vortex states.

DOI: 10.1103/PhysRevD.109.096015

I. INTRODUCTION

In the vast majority of cases, it is enough to calculate particle interactions using the plane-wave approximation. Nevertheless, many studies have shown that the non-plane-wave nature of particles plays an important role in physical processes. For example, the so-called MD effect, which reveals the importance of the impact parameter, can only be explained when describing particles as wave packets rather than plane waves [1,2]. The so-called "beam size effect" reveals that the size of the particles cannot be neglected when it is comparable to or smaller than the particle Compton wavelength [3–6]. Also, vortex particle collisions exhibit peculiar features which cannot be found in the plane-wave approximation [7,8]. In this paper, we will demonstrate yet another special feature arising in two-vortex-state collisions which has no counterpart for plane-wave scattering.

Vortex states have quantized intrinsic angular momentum, which is different from spin. They are characterized by a spiral phase front which is described by the extra phase factor $e^{i\ell\varphi}$, where ℓ is called the topological charge and is proportional to the orbital angular momentum. Several kinds of particles prepared in such a state have been experimentally produced: photons [9], electrons [10], neutrons [11], and small atoms [12]. They have found applications in fields such as manipulation of atoms [13–15], quantum communication [16–19], microscopy [20], and so on. Along with the generation of vortex particles, the study of particle interactions involving vortex states attracts a lot of attention [8]. Many processes involving vortex particles have been studied—for example, vortex particle propagation in electromagnetic fields [21–23], vortex particle scattering by a target [24–26], decay of the vortex muons [27,28], photo-induced processes initiated by vortex photons [29–31], and so on. There are also several studies focusing on the collision of two vortex particles [32–34]. A key characteristic of two-vortex-particle collisions is a peculiar oscillatory dependence of the differential cross section on the transverse momentum. This sort of oscillation depends on the topological charges of the initial vortex states. However, so far, this dependence has only been discussed with Bessel vortex states, which are not physical because they cannot be normalized in the transverse space. A physical vortex state can have longitudinal momentum uncertainty and an energy spread. Thus, the physical vortex states collision may result in special longitudinal momentum or energy distributions. The dependence of these distributions on the topological charge is not immediately clear.

In this paper, we clarify this issue. To this end, we study the collisions of two vortex particles in three different cases: when they are prepared in the Bessel vortex state, in a general monochromatic vortex state, and in the Laguerre-Gaussian vortex state. Transverse, longitudinal, and energy distributions are calculated. We compare the three cases and find general topological features which depend on the topological charges of the two initial vortex states. To keep the discussion clear, we consider collisions in the scalar ϕ^4 theory.

The paper is organized as follows: In Sec. II, we present calculations of the transition amplitude $\mathcal{S}$ for the three different cases. In Sec. III, we discuss and compare the resulting total final-momentum distributions. In Sec. IV, we

*zhaopch5@mail2.sysu.edu.cn

draw conclusions. In this paper, all the three-dimensional vectors are expressed using bold letters.

II. COLLISION OF TWO VORTEX STATES

In this study, we only consider central collisions of vortex states that carry quantized orbital angular momenta along their propagation direction, which we label as the z axis. This means that the vortex states are eigenstates of the z component of the angular momentum operator. Central collisions of these eigenstates must produce the total final-momentum distribution, which is rotational-symmetric around the axis z, if we measure the final states in 3-momentum basis—i.e., plane-wave basis. In this kind of distribution, we have the freedom to choose the transverse axes; we select the axis x along the transverse part of the total final momentum.

A. Bessel vortex collision

A Bessel vortex state is characterized by three quantum numbers: the energy E, the longitudinal momentum p_z, and the topological charge ℓ, which can only be an integer. The Bessel state cannot be normalized in the transverse plane. The momentum-space distribution of this state is just a circle orthogonal to the axis z. The momenta of all the plane-wave components inside the Bessel state form a cone, whose base is just this circle. The state propagating along the z direction is described by the wave function

$$\psi^B_{E,p_z,\ell}(\mathbf{x},t) = \int \frac{d^3\mathbf{k}}{(2\pi)^3} a^B_{p_z\ell}(\mathbf{k}) \exp(i\mathbf{k}\mathbf{x} - iEt),$$
$$a^B_{p_z\ell}(\mathbf{k}) = N^B \delta(k_\perp - \kappa)\delta(k_z - p_z)\exp(i\ell\varphi_{\mathrm{k}}), \qquad (1)$$

where $E = \sqrt{\mathbf{k}^2 + m^2}$ is the energy of the plane wave with momentum $\mathbf{k}$ and mass m, $\kappa = \sqrt{\mathbf{k}^2 - p_z^2}$ is the modulus of the transverse momentum, and φ_k is the azimuthal angle of this plane wave. N^B is the normalization coefficient, but we will not need its explicit expression.

Being different from the plane-wave particle interactions, the collisions of two Bessel vortex states show some new features that can be observed, including non-constant total transverse momentum and the oscillatory transverse momentum distribution [8,34]. The new distributions represent new physical observables which are absent in traditional collision kinematics. The momnetum-space oscillations appear because of interference between different plane-wave components present in the initial vortex states. For non-plane-wave-state collisions, "interference" means that we can find multiple initial plane-wave combinations which lead to the same final state. For Bessel vortex state collisions, this interference involves only two isolated points in momentum space, as shown in Fig. 1. In this figure, we draw the interference scheme in the transverse plane of momentum space at fixed total final transverse momentum, since the total longitudinal momentum is fixed by itself. $\vec{q}_\perp$ is the total final transverse momentum, while $\vec{k}_{1\perp}$ and $\vec{k}_{2\perp}$ label the transverse momenta of plane-wave components in the two initial vortex states. Two circles with centers located at the end points of vector $\vec{q}_\perp$ are drawn in the figure. The upper green circle with radius κ_2 is the momentum distribution of all $(\vec{q}_\perp - \vec{k}_{2\perp})$'s, and the lower blue circle with radius κ_1 is the momentum distribution of all $\vec{k}_{1\perp}$'s. The two circles intersect at two red points, which satisfy the conservation law: $\vec{q}_\perp = \vec{k}_{1\perp} + \vec{k}_{2\perp}$. They show clearly the two interference paths in which the plane-wave momenta are named with the subscripts "a" and "b." In principle, $\vec{q}_\perp$ can be chosen at will, as long as it satisfies

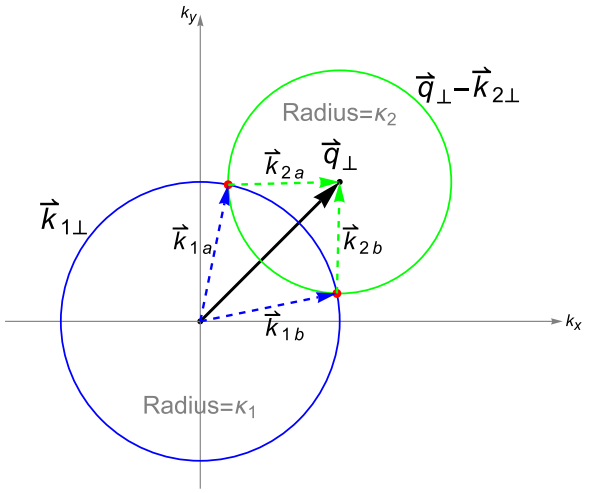

FIG. 1. Interference scheme for a Bessel vortex states collision at fixed total transverse momentum $\vec{q}_\perp$. Two circles intersect at two red points, which correspond to two interference paths. The momentum combinations of the two paths are labeled with the subscripts "a" and "b." The interference is discussed in the transverse plane of momentum space, since the longitudinal momenta are fixed. The transverse momentum of the plane-wave components in one initial vortex state is $\vec{k}_{1\perp}$; the other is $\vec{k}_{2\perp}$. The momentum distribution of all $\vec{k}_{1\perp}$'s forms the blue circle with radius κ_1, and the momentum distribution of all $(\vec{q}_\perp - \vec{k}_{2\perp})$'s forms the green circle with radius κ_2.

$$|\kappa_1 - \kappa_2| < |\vec{q}_\perp| < |\kappa_1 + \kappa_2|.$$

For convenience, we choose the direction of $\vec{q}_\perp$ to be the same as the k_x axis in the following calculation. In this setting, $\vec{q}_\perp = (q_\perp, 0)$, where $q_\perp$ is the modulus of the vector.

The $\mathcal{S}$-matrix element for the process "two Bessel vortex states to two plane-wave states" has been studied in Ref. [32]. Here, we review it again. For convenience, we choose the azimuth angle of $\mathbf{q}$ to be $\varphi_q = 0$, which means that $\vec{q}_\perp$ lies on the k_x axis. In this special case, the transition amplitude is

$$\begin{aligned}\mathcal{S}(B_1+B_2\to P_3+P_4) &\propto \int d^3\mathbf{k}_1 d^3\mathbf{k}_2 a^B_{p_{1z}\ell_1}(\mathbf{k}_1) a^B_{p_{2z}\ell_2}(\mathbf{k}_2)\mathcal{M}\delta^3(\mathbf{k}_1+\mathbf{k}_2-\mathbf{q})\delta(E_1+E_2-E_q)\\ &\propto \int_0^{2\pi} d\varphi_1 \int_0^{2\pi} d\varphi_2 e^{i(\ell_1\varphi_1+\ell_2\varphi_2)}\delta^2(\vec{k}_{1\perp}+\vec{k}_{2\perp}-\vec{q}_\perp)\delta(p_{1z}+p_{2z}-q_z)\delta(E_1+E_2-E_q)\\ &\propto \frac{\cos(\ell_1\varphi_{1a}+\ell_2\varphi_{2a})}{\Delta}\delta(p_{1z}+p_{2z}-q_z)\delta(E_1+E_2-E_q),\end{aligned} \tag{2}$$

where the subscripts 1 and 2 represent the two initial states, φ_i $(i=1,2)$ is the azimuth angle of momentum $\vec{k}_{i\perp}$, φ_{ia} is the azimuth angle of momentum $\vec{k}_{ia}$, E_q is the total energy of the final state, and

$$\Delta=\sqrt{(\kappa_1+\kappa_2+q_\perp)(\kappa_1-\kappa_2+q_\perp)(-\kappa_1+\kappa_2+q_\perp)(\kappa_1+\kappa_2-q_\perp)}$$

is the area of the triangle lying in the transverse plane formed by $(\kappa_1,\kappa_2,q_\perp)$. From the second line of Eq. (2) to the third line, we have used the equation

$$\int_0^{2\pi} d\varphi_1 \int_0^{2\pi} d\varphi_2 \delta^2(\vec{k}_{1\perp}+\vec{k}_{2\perp}-\vec{q}_\perp) f(\varphi_1,\varphi_2)=\frac{f(\varphi_{1a},\varphi_{2a})+f(\varphi_{1b},\varphi_{2b})}{\Delta},$$

which is acquired in Ref. [32]. The azimuth angles with the subscripts "a" and "b" correspond to the two different paths shown in Fig. 1. We also define the topological charges according to a single z axis, even though the two particles are counterpropagating, noting that it is a pointlike interaction with a momentum-independent interaction parameter for a $2\to 2$ process in scalar ϕ^4 theory if we only consider tree-level diagrams. Hence, the calculation from the second line of Eq. (2) to the third line is correct. In the third line of Eq. (2), φ_{ia} is dependent on $q_\perp$:

$$\varphi_{1a}=\arccos\left(\frac{\kappa_1^2+q_\perp^2-\kappa_2^2}{2q_\perp\kappa_1}\right),$$
$$\varphi_{2a}=-\arccos\left(\frac{\kappa_2^2+q_\perp^2-\kappa_1^2}{2q_\perp\kappa_2}\right).$$

From Eq. (2), we see that the collision of two Bessel vortex states can only generate final states that have the fixed total energy $E_1+E_1=E_q$ and the fixed longitudinal momentum $k_{1z}+k_{2z}=q_z$. However, the total final transverse momentum $q_\perp$ is not fixed, but is distributed within the region

$$|\kappa_1-\kappa_2|<q_\perp<|\kappa_1+\kappa_2|,$$

and the scattering matrix amplitude exhibits an oscillatory behavior in this range.

B. General monochromatic vortex collision

A general monochromatic vortex state can be written as a superposition of many Bessel vortex states with the same energy. It has two quantum numbers: the energy E and the topological charge ℓ. It can be normalized in the transverse plane. In momentum space, all the plane-wave components have momenta lying on a sphere of radius $k\equiv|\mathbf{k}|$ and are accompanied by different weighting factors. The state propagating along the z direction is described by the wave function

$$\begin{aligned}\psi^M_{E,\ell}(\mathbf{x},t) &= \int \frac{d^3\mathbf{k}}{(2\pi)^3} a^M_\ell(\mathbf{k})\exp(i\mathbf{k}\mathbf{x}-iEt),\\ a^M_\ell(\mathbf{k}) &= N^M f(\theta)\delta(\sqrt{\mathbf{k}^2+m^2}-E)\exp(i\ell\varphi_{\mathrm{k}}),\end{aligned} \tag{3}$$

where θ is the polar angle of the momentum $\mathbf{k}$, and N^M is the normalization coefficient of the state. Note that $f(\theta=0)=f(\theta=\pi)=0$ to avoid phase singularity. In realistic situations, f should be concentrated in a narrow region of θ. For the numerical calculations, we use

$$f(\theta)=\sin\theta\exp\left[-\frac{(\theta-\theta_0)^2}{\sigma_0^2}\right], \tag{4}$$

where θ_0 and σ_0 are small constants.

For a fixed total final 4-momentum, there are many plane-wave combinations that satisfy the energy-momentum conservation law and lead to the same final state. A schematic analysis of the contributions in momentum space is shown in Fig. 2. The red circle, which is the intersection of the two spheres, is perpendicular to the total final momentum $\mathbf{q}$ and displays all points which can lead to the same final state. One sphere shows the $\mathbf{k}_1$ distribution and another displays the $(\mathbf{q}-\mathbf{k}_2)$ distribution, where $(\mathbf{k}_1,\mathbf{k}_2)$ represent momentum components in the two initial vortex states. Only intersection points are selected by the conservation law. Since the momenta of the initial vortex states are concentrated within certain bands as shown in Eq. (4), the main contribution to the production amplitude comes from the intersection of the red circle with

two colored bands, noting that $\mathbf{q}$ is positioned along the k_x axis and $|\mathbf{k}_1| = |\mathbf{k}_2|$ in the figure. These are convenient for illustration but do not represent general cases. In principle, $\mathbf{q}$ can be chosen arbitrarily as long as it satisfies the condition

$$||\mathbf{k}_1| - |\mathbf{k}_2|| < |\mathbf{q}| < ||\mathbf{k}_1| + |\mathbf{k}_2||,$$

and $\mathbf{k}_1$, $\mathbf{k}_2$ can be arbitrary.

The $\mathcal{S}$-matrix element for the process "two monochromatic vortex states to two plane-wave states" is

$$\begin{aligned}\mathcal{S}(M_1 + M_2 \to P_3 + P_4) &\propto \int d^3\mathbf{k}_1 d^3\mathbf{k}_2 a^M_{\ell_1}(\mathbf{k}_1) a^M_{\ell_2}(\mathbf{k}_2) \mathcal{M}\delta^{(3)}(\mathbf{k}_1 + \mathbf{k}_2 - \mathbf{q})\delta(E_1 + E_2 - E_q) \\ &\propto \int_0^\pi d\hat{\varphi}_1 \frac{k_1 k_2}{q} f_1(\theta_1) f_2(\theta_2) \cos(\ell_1\varphi_1 + \ell_2\varphi_2)\mathcal{M}\delta(E_1 + E_2 - E_q), \end{aligned} \tag{5}$$

where k_1, k_2, and q are modulus of the momenta $\mathbf{k}_1$, $\mathbf{k}_2$, and $\mathbf{q}$.

We utilize two coordinate systems in this integral to facilitate calculations. In the first system, we utilize unhatted coordinates. In the second system, coordinates are denoted with hats. The variables $(\theta_i, \varphi_i, i = 1, 2)$ represent the polar angle and azimuthal angle in the first coordinate system, while $(\hat{\theta}_i, \hat{\varphi}_i)$ denote their counterparts in the second coordinate system. The relationship between the two coordinate systems is a straightforward rotation in the $k_x O k_z$ plane, as illustrated in Fig. 3. Momentum $\mathbf{p}$ in the two systems is related by the transformation

$$\begin{pmatrix} \hat{p}_x \\ \hat{p}_y \\ \hat{p}_z \end{pmatrix} = \begin{pmatrix} \cos\theta_q & 0 & -\sin\theta_q \\ 0 & 1 & 0 \\ \sin\theta_q & 0 & \cos\theta_q \end{pmatrix} \begin{pmatrix} p_x \\ p_y \\ p_z \end{pmatrix},$$

where θ_q is the angle between the vector $\mathbf{q}$ and the k_z axis.

In the second line of Eq. (5), the values (θ_i, φ_i) depend on $(q, \theta_q, \hat{\varphi}_i)$:

$$\varphi_i = \arccos\left(\frac{\cos\hat{\theta}_i \sin\theta_q + \sin\hat{\theta}_i \cos\theta_q \cos\hat{\varphi}_i}{\sqrt{1 - (\cos\hat{\theta}_i \cos\theta_q - \sin\hat{\theta}_i \sin\theta_q \cos\hat{\varphi}_i)^2}}\right),$$

$$\theta_i = \arccos(\cos\hat{\theta}_i \cos\theta_q - \sin\hat{\theta}_i \sin\theta_q \cos\hat{\varphi}_i),$$

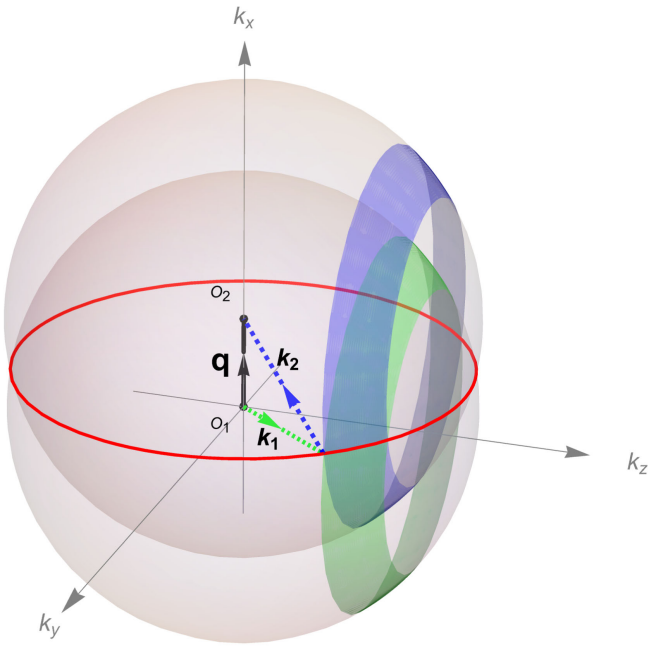

FIG. 2. Interference scheme for the general monochromatic vortex states collision. Two momentum spheres intersect at points which result in the same total final momentum $\mathbf{q}$. They form the red circle. The momentum of the plane-wave components in one initial vortex state is denoted as $\mathbf{k}_1$, while in another state it is denoted as $\mathbf{k}_2$. The momentum distribution of all $\mathbf{k}_1$'s forms the lower sphere, and the distribution of all $(\mathbf{q} - \mathbf{k}_2)$'s forms the upper sphere. The two girdles in the two spheres represent the primary contributions of the two initial vortex states. The intersection of the red circle with the two girdles indicates the main contribution points to the fixed final state. It is important to note that the choice of $\mathbf{q}$ along the k_x axis and $|\mathbf{k}_1| = |\mathbf{k}_2|$ are not general cases.

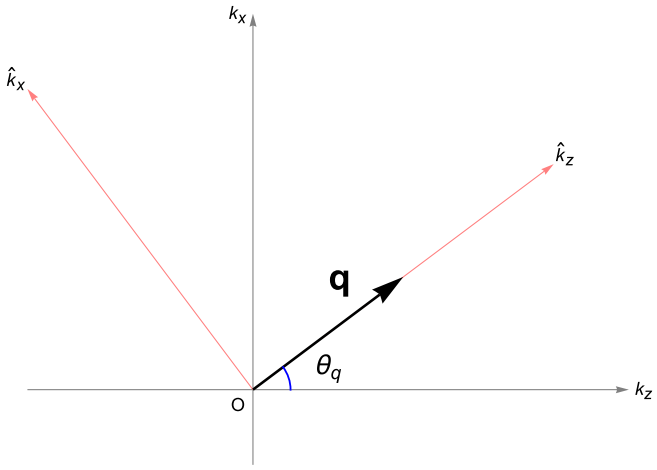

FIG. 3. Two coordinate systems in momentum space for Eq. (5). One is denoted with hats to distinguish it from the other. Here, the k_y axis is not changed, and the $k_x O k_z$ plane is rotated counterclockwise by an angle θ_q to yield the $\hat{k}_x O \hat{k}_z$ plane.

and

$$\hat{\varphi}_2 = -\hat{\varphi}_1,$$
$$\hat{\theta}_1 = \arccos\left(\frac{k_1^2 + q^2 - k_2^2}{2qk_1}\right),$$
$$\hat{\theta}_2 = \arccos\left(\frac{k_2^2 + q^2 - k_1^2}{2qk_2}\right).$$

Thus, once the integral in Eq. (5) is integrated out, we can obtain the result as a function of vector $\mathbf{q}$.

Collisions of two monochromatic vortex states can only generate final states with a fixed energy; this is also shown by the energy delta function in Eq. (5). However, the total transverse and longitudinal momentum distributions span nonzero ranges, and within these regions, they exhibit oscillations.

C. Laguerre-Gaussian vortex collision

The Laguerre-Gaussian vortex state can also be written as a superposition of many Bessel vortex states. It is not a monochromatic state. It can be well normalized on the transverse plane. It has two quantum numbers, which are the topological charge ℓ and principal quantum number n, both of which must be integers. In momentum space, all the momentum components contribute to it. The state propagating along the z direction is described by the wave function

$$\psi^L_{n,\ell}(\mathbf{x}, t) = \int \frac{d^3\mathbf{k}}{(2\pi)^3} a^L_{n\ell}(\mathbf{k}) \exp(i\mathbf{k}\mathbf{x} - iEt),$$
$$a^L_{n\ell}(\mathbf{k}) = N^L k_\perp^{|\ell|} L_n^{|\ell|}\left(\frac{k_\perp^2}{\sigma_\perp^2}\right) \times \exp\left(-\frac{k_\perp^2}{2\sigma_\perp^2} - \frac{(k_z - \bar{k}_z)^2}{2\sigma_z^2} + i\ell\varphi_k\right), \quad (6)$$

where N^L is the normalization coefficient, $k_\perp$ is the modulus of $\mathbf{k}$'s transverse part, $\sigma_\perp$ and σ_z determine the transverse and longitudinal sizes of the state, $\bar{k}_z$ is the average longitudinal momentum, and L_n is the generalized Laguerre polynomial.

For a fixed total final 4-momentum $(E_q, \mathbf{q})$, the conservation of 3-momentum requires that the momenta $\mathbf{q}$, $\mathbf{k}_1$, and $\mathbf{k}_2$ form a triangle, while the conservation of energy tells us $E_q = \sqrt{k_1^2 + m_1^2} + \sqrt{k_2^2 + m_2^2}$. These two conditions define a closed two-dimensional surface in momentum space.

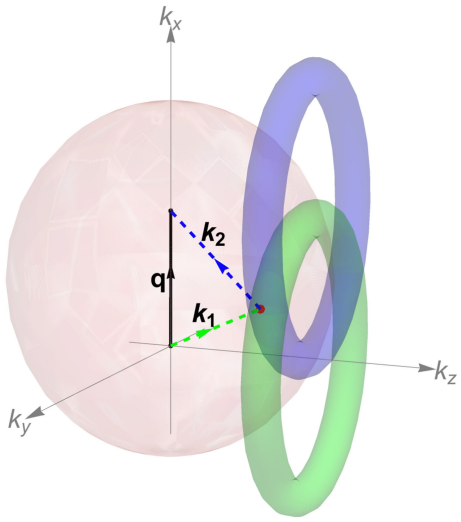

FIG. 4. Interference scheme for a Laguerre-Gaussian vortex states collision. The surface of an ellipsoid, with its foci located at the end points of vector $\mathbf{q}$, represents all the points that yield the same total momentum and energy. The two doughnuts in the two spheres represent the primary contributions of the $(\mathbf{q} - \mathbf{k}_2)$ and $\mathbf{k}_1$ distributions. The intersection of the ellipsoid surface with the two doughnuts indicates the main contribution points to the fixed final state. It is important to note that the choice of $\mathbf{q}$ along the k_x axis is not a general case. In addition, the central values of the momenta for two initial states have the same modulus in the figure, which is also not a general case. Here, we ignore the mass of the particles ($m = 0$).

Specially, for the zero-mass case, it is an ellipsoid. A schematic analysis of interference space is displayed in Fig. 4 for the zero-mass case. All the contribution points lie on an pink ellipsoid whose focal points happen to be end points of vector $\mathbf{q}$. The $(\mathbf{q} - \mathbf{k}_2)$ and $\mathbf{k}_1$ distributions concentrate on two doughnuts. The main contribution to the final state lies on the intersection of the ellipsoid with the two doughnuts—note that $\mathbf{q}$ is positioned along the k_x axis in the figure. In addition, the central values of the momenta for the two initial states are chosen to have the same modulus. These are convenient for illustration but do not represent general cases. In principle, $\mathbf{q}$ and the central values of the momenta for the two initial states can be chosen arbitrarily.

The $\mathcal{S}$-matrix element for the process "two Laguerre-Gaussian vortex states to two plane-wave states" is

$$\mathcal{S}(L_1 + L_2 \to P_3 + P_4) \propto \int d^3\mathbf{k}_1 d^3\mathbf{k}_2 a^L_{n\ell_1}(\mathbf{k}_1) a^L_{n\ell_2}(\mathbf{k}_2) \mathcal{M} \delta^3(\mathbf{k}_1 + \mathbf{k}_2 - \mathbf{q}) \delta(E_1 + E_2 - E_q)$$
$$\propto \int_0^\pi d\hat{\varphi}_1 \int_0^\pi d\hat{\theta}_1 \frac{\sin\hat{\theta}_1 k_1^2 E_1 E_2 g_1(k_{1\perp}, k_{1z}) g_2(k_{2\perp}, k_{2z})}{|E_q k_1 - E_1 q \cos\hat{\theta}_1|} \cos(\ell_1\varphi_1 + \ell_2\varphi_2)\mathcal{M}, \quad (7)$$

where

$$g_i(k_{i\perp},k_{iz})=k_{i\perp}^{|\ell_i|}L_{n_i}^{|\ell_i|}\left(\frac{k_{i\perp}^2}{\sigma_{i\perp}^2}\right)\exp\left(-\frac{k_{i\perp}^2}{2\sigma_{i\perp}^2}-\frac{(k_{iz}-\bar{k}_{iz})^2}{2\sigma_{iz}^2}-iE_it\right),\qquad k_{i\perp}=k_i\sin\theta_i,\qquad k_{iz}=k_i\cos\theta_i,\quad i=1,2.$$

We also use two sets of coordinate systems, which are the same as those used in the monochromatic vortex collision case. In the second line of Eq. (7), (k_i,φ_i,θ_i) are dependent on $(E_q,q,\theta_q,\hat{\varphi}_1,\hat{\theta}_1)$. In the zero-mass case, the relations are

$$k_1=\frac{E_q^2-q^2}{2(E_q-q\cos\hat{\theta}_1)},$$
$$k_2=E_q-k_1,$$
$$\varphi_i=\arccos\left(\frac{\cos\hat{\theta}_i\sin\theta_q+\sin\hat{\theta}_i\cos\theta_q\cos\hat{\varphi}_i}{\sqrt{1-(\cos\hat{\theta}_i\cos\theta_q-\sin\hat{\theta}_i\sin\theta_q\cos\hat{\varphi}_i)^2}}\right),$$
$$\theta_i=\arccos(\cos\hat{\theta}_i\cos\theta_q-\sin\hat{\theta}_i\sin\theta_q\cos\hat{\varphi}_i),$$

where θ_q is the angle between the vector $\mathbf{q}$ and the z axis, and

$$\hat{\varphi}_2=-\hat{\varphi}_1,$$
$$\hat{\theta}_2=\arccos\left(\frac{k_2^2+q^2-k_1^2}{2qk_2}\right).$$

From Eq. (7), we see that there is no limitation on the final total momentum or energy for the collision of two Laguerre-Gaussian vortex states. Oscillation may appear in the transverse distribution, longitudinal distribution, and energy distribution, with E_q, q, and θ_q varying.

III. RESULTS

All the results shown below are based on the simple ϕ^4 scalar model with a constant amplitude $\mathcal{M}$ in tree level. For definiteness, we assume that the two colliding vortex states have the same momentum distributions except for different topological charges.

A. Bessel vortex collision

For the Bessel state collision, the total final energy and longitudinal momentum are fixed by the initial states, which is revealed by delta functions in Eq. (2). Thus, we only show radial transverse distributions within the range $|\kappa_1-\kappa_2|<q_\perp<|\kappa_1+\kappa_2|$, considering that the distributions must be azimuthally symmetric. The value of $|\mathcal{S}|$ exhibits oscillations as a function of $q_\perp$ due to the factor $\cos(\ell_1\varphi_1+\ell_2\varphi_2)$. This oscillatory behavior can be seen as a momentum-space analogue of the famous two-slit interference pattern [34].

The value of $|\mathcal{S}|$ diverges near the boundaries of the $q_\perp$ region due to the denominator Δ in Eq. (2). This unphysical behavior is the result of the initial Bessel states being non-normalizable in the transverse plane. Nevertheless, we still use Bessel states for comparison, because they are a reasonable starting point for the description of realistic

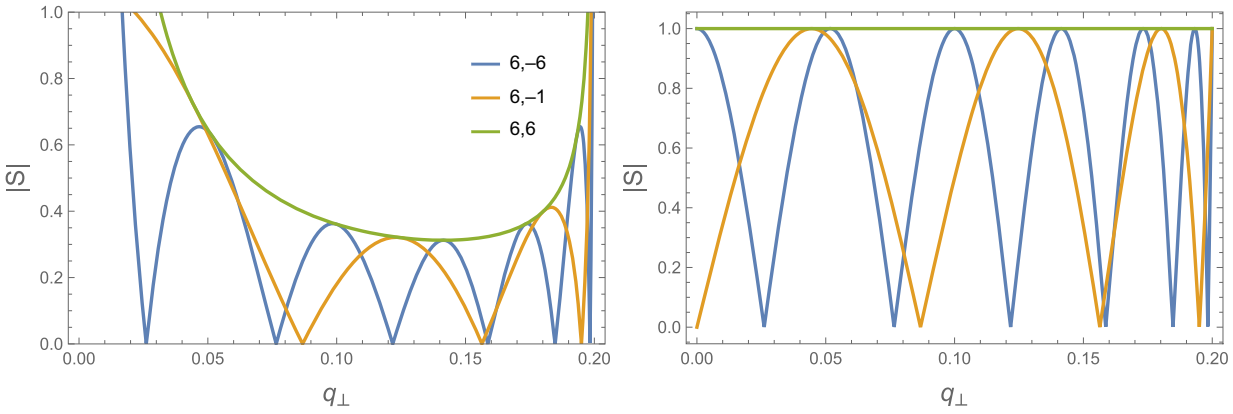

FIG. 5. One-dimensional oscillation pattern of the $|\mathcal{S}|$ distribution for a Bessel vortex states collision. The distributions have been normalized so that the biggest value of the vertical coordinate is 1. Left: $|\mathcal{S}|$ oscillates when the total final transverse momentum $q_\perp$ changes. Right: $\Delta\cdot|\mathcal{S}|$ oscillates when $q_\perp$ changes. The oscillation frequency is dependent on initial topological charges. Here, the three lines correspond to three cases that differ only by topological charges (blue for $\ell_1=6$; $\ell_2=-6$, brown for $\ell_1=6$, $\ell_2=-1$; green for $\ell_1=6$, $\ell_2=6$). Other parameters of initial states: $E_1=E_2=2$ MeV, $\kappa_1=\kappa_2=0.1$ MeV. Divergences have been cut out.

vortex states, just as the traditional plane waves are a good approximation of realistic wave packets.

Examples of the oscillation pattern are shown in Fig. 5, and they confirm the above discussion. To demonstrate the oscillations more clearly, in the right plot we remove the divergence-inducing denominator Δ.

For future discussion, it is convenient to pay attention to the points in momentum space where $|\mathcal{S}|$ passes through zero. In the present example, we have several zero points, which break the entire $q_\perp$ domain into disjoint intervals. The number n^B of these intervals is completely determined by the initial topological charges:

$$n^B = \text{Integer}[|\ell_1 - \ell_2|/2 + 1].$$

Will this expression, which we derived for the Bessel states, remain the same if we use other forms of vortex states with the same ℓ? The answer is negative, which we will verify in the following sections.

B. General monochromatic vortex collision

For a general monochromatic vortex collision, only the total final energy is fixed by initial states, as the delta function in Eq. (2) reveals. Thus, we will get both the

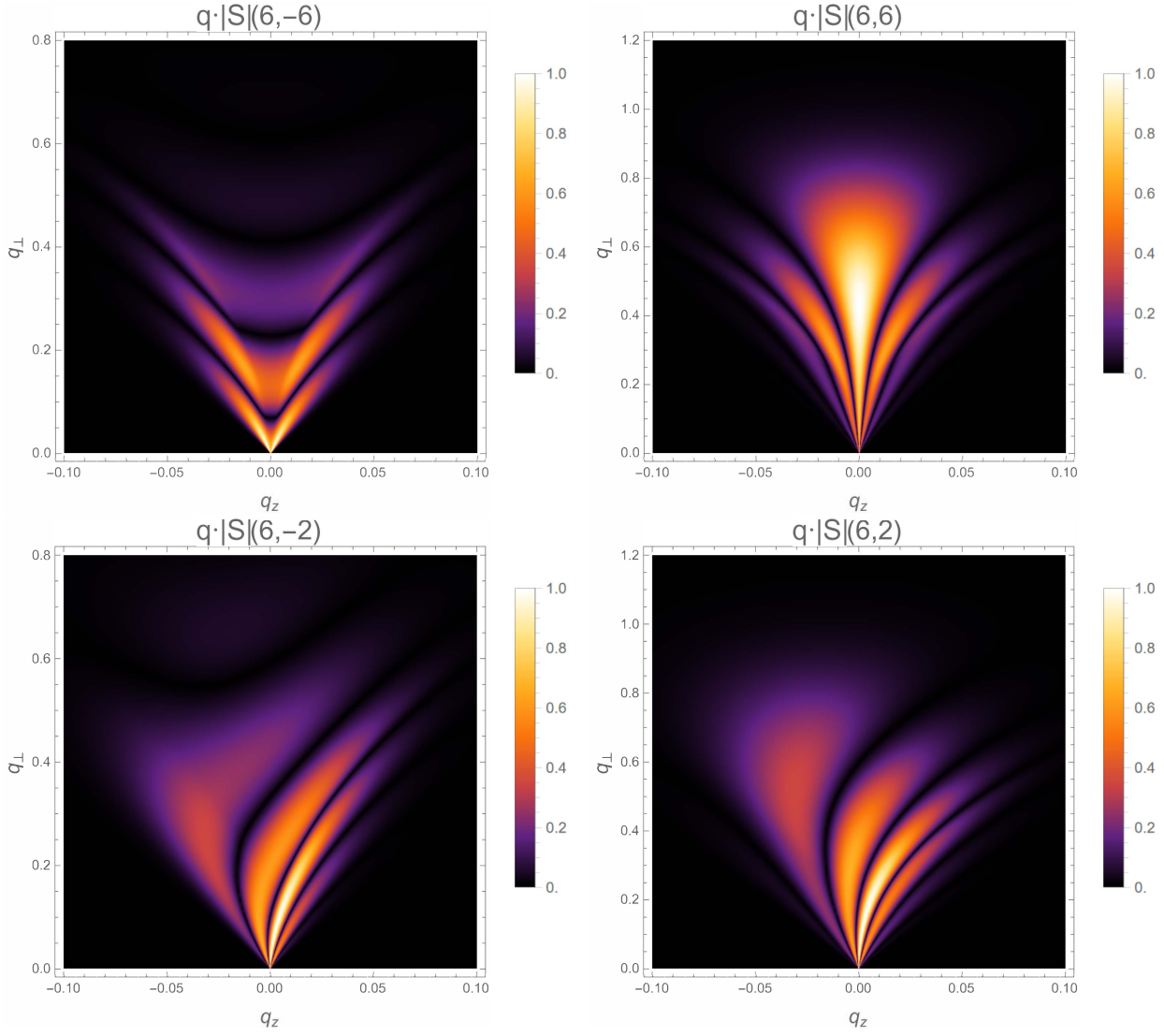

FIG. 6. Two-dimensional oscillation pattern of a $q \cdot |\mathcal{S}|$ distribution for the general monochromatic vortex states collision. The distribution has been normalized so that its biggest value is 1. We set $(\ell_1 = -\ell_2 = 6)$ for the top-left picture, $(\ell_1 = \ell_2 = 6)$ for the top-right picture, $(\ell_1 = 6, \ell_2 = -2)$ for the bottom-left picture, and $(\ell_1 = 6, \ell_2 = 2)$ for the bottom-right picture. Other parameters of initial states: $E_1 = E_2 = 2$ MeV, $\theta_{01} = \theta_{02} = \sigma_{01} = \sigma_{02} = 0.1$ rad.

transverse and longitudinal distributions. The two-dimensional distribution has oscillatory behavior, which depends on the topological charges of the initial states. The boundary of the distribution is determined by the momentum modulus (i.e., the radius of the momentum distribution sphere) of the two states: $||\mathbf{k}_1| - |\mathbf{k}_2|| < q < ||\mathbf{k}_1| + |\mathbf{k}_2||$. The oscillation seems to be an analogue to the Fresnel diffraction in momentum space, since the interference region is a circle, as Fig. 2 shows. But, at different points on the circle, weight factors are different. Thus, it is actually an analogue to the case in which the Fresnel diffraction experiment is prepared with an inhomogeneous wave source.

As the factor $1/q$ in Eq. (5) reveals, the $|\mathcal{S}|$ distribution is highly concentrated near the point $q = 0$. The asymptotic behavior at this value is

$$\lim_{q\to 0}|\mathcal{S}| = \begin{cases} \infty & \text{if } \ell_1 + \ell_2 \equiv 0, \\ 0 & \text{if } \ell_1 + \ell_2 \neq 0. \end{cases}$$

The divergence is a direct result of the non-normalizable initial states. They can be normalized in the transverse plane but cannot be normalized in the longitudinal direction. This means the state can be seen as a beam state, but not a particle state. To see clearly the oscillatory behavior, we will show $q \cdot |\mathcal{S}|$ instead of the $|\mathcal{S}|$ distribution. It rearranges

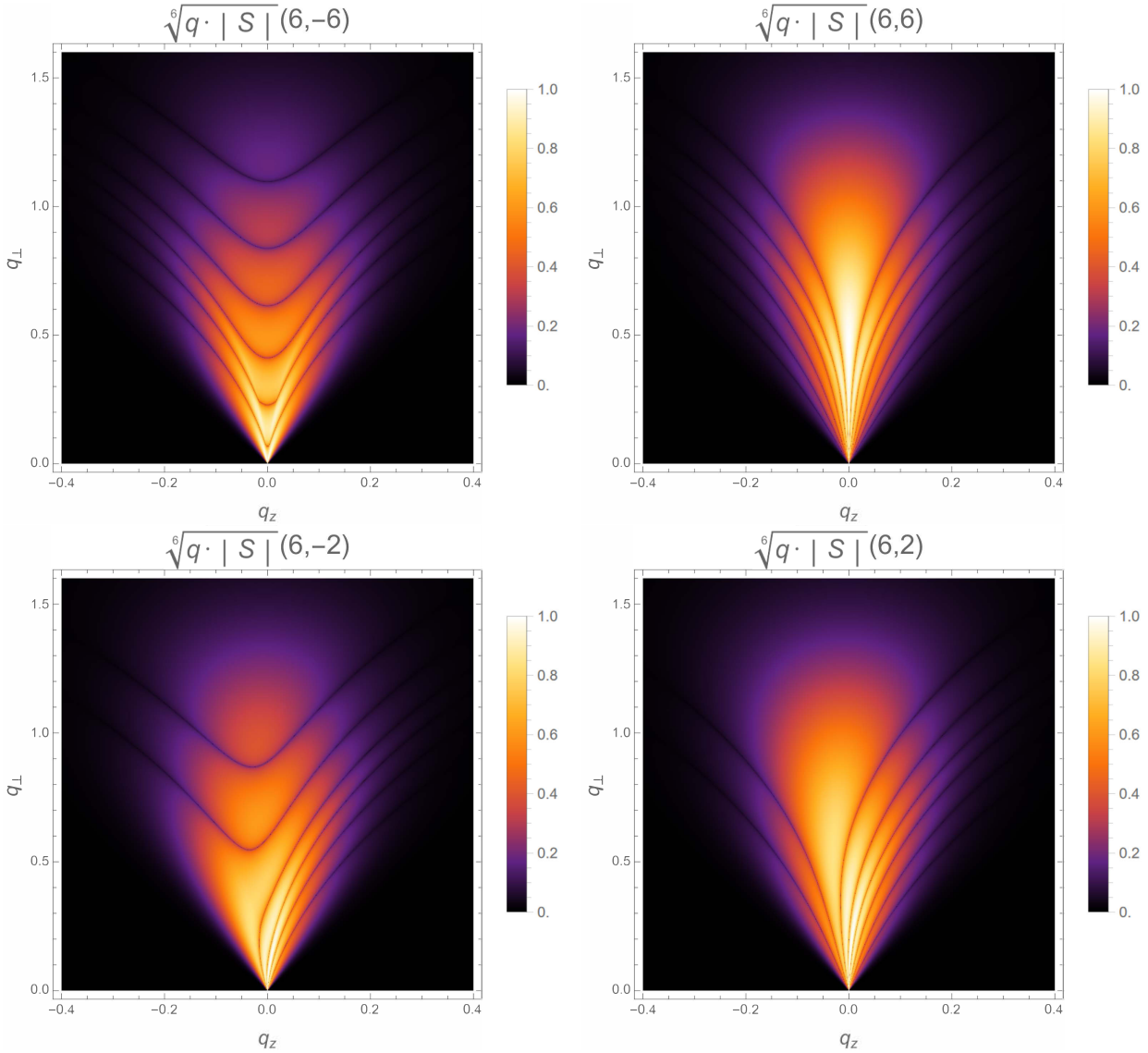

FIG. 7. Two-dimensional oscillation patterns of a $\sqrt[6]{q\cdot|\mathcal{S}|}$ distribution for the general monochromatic vortex states collision. The distribution has been normalized so that its biggest value is 1. We set $(\ell_1 = -\ell_2 = 6)$ for the top-left picture, $(\ell_1 = \ell_2 = 6)$ for the top-right picture, $(\ell_1 = 8, \ell_2 = -4)$ for the bottom-left picture, and $(\ell_1 = 8, \ell_2 = 4)$ for the bottom-right picture. Other parameters of initial states: $E_1 = E_2 = 2$ MeV, $\theta_{01} = \theta_{02} = \sigma_{01} = \sigma_{02} = 0.1$ rad.

the distribution but will not influence oscillatory behavior. The results are shown in Fig. 6. Two-dimensional oscillation patterns show that the distribution oscillates not only with the transverse momentum changing, but also with the longitudinal momentum changing. This is a new feature that is completely different with the Bessel vortex case. This appears because the interference space (the circle shown in Fig. 2) includes points with both different transverse momentum and different longitudinal momentum.

Another important result is that the oscillation pattern is partly smeared out after integration in Eq. (5). There is the obvious tendency that the values of bright oscillation peaks decrease, and some peaks may just run out of our sight with much smaller amplitudes. A more careful treatment does find more peaks and will be shown later. The smeared-out result is analogous to the smeared-out pattern in multifrequency double-slit interference [35]. Due to the energy dispersion of initial states, some of the bright peaks in the final interference pattern significantly decrease and seem to disappear. In fact, the interference space shown in Fig. 2 can be seen as the combination of many "two-slits," which are characterized by different θ's. By the weight function [Eq. (4)], all the "two-slits" are assigned with different weight factors, and the final interference pattern is partly smeared out.

There is an interesting result: the interference pattern is symmetric under the reverse of longitudinal momentum (or forward-backward symmetric) if the topological charges of initial states have the same absolute values. Otherwise, it will be forward-backward asymmetric. This is different in the Bessel vortex collision case, in which asymmetric information that is only induced by two topological charges cannot be reserved in the final distribution. However, the asymmetric information that is only induced by the sign of topological charges cannot be kept. This is not difficult to understand. Three kinds of transformations should be considered here: parity transformation in the z direction, the reverse of topological charges, and parity transformation in the transverse plane along any direction. For initial states which satisfy $|\ell_1| = |\ell_2|$, the first transformation is equivalent to the second one, which is equivalent to the third one. Since we are only interested in a rotational-symmetric total final-momentum distribution which does not change under the reverse of transverse momentum in any direction, it should also be symmetric when we reverse the longitudinal momentum. For the case $|\ell_1| \neq |\ell_2|$, the first transformation is not equivalent to the second one.

The most attractive feature for the collision of two general monochromatic vortex states lies in distributions that are reshaped by the nth root, which are shown in Fig. 7. Only four examples are shown in this figure, and more examples will be listed in Fig. 10 in the Appendix. All the $q \cdot |\mathcal{S}|$ values are redefined by the "nth root," except for zeros. Thus, we can see all the unconnected areas, which are partitioned by zero lines, in the distribution, and find special topological structures that are completely dependent on initial topological charges. The number of unconnected areas can be expressed as a function of initial topological charges:

$$n^M = n_\perp^M + n_z^M - 1, \quad n_\perp^M = \frac{|\ell_1| + |\ell_2| - |\ell_1 + \ell_2|}{2} + 1,$$
$$n_z^M = |\ell_1 + \ell_2| + 1.$$

The superscript "M" represents initial general monochromatic vortex states, and n^M is the total number. According to transverse and longitudinal oscillation, two other kinds of numbers, $n_\perp^M$ and n_z^M, are defined. They correspond to the count area numbers in the transverse and longitudinal directions, respectively. The decomposition of topological numbers seems to be nonsense now. Meanwhile, it will make sense after comparison with the Laguerre-Gaussian vortex collision case.

C. Laguerre-Gaussian vortex collision

For a Laguerre-Gaussian vortex collision, we can get not only the total momentum distribution in the transverse and longitudinal directions, but also the total energy distribution of final plane waves. There is no certain boundary for the distribution, since momentum components of initial states run out of all the momentum space, though some of them are more probable than others. The interference region is an ellipsoid, and there is no analogue to this kind of interference.

Two-dimensional distributions in the xOy plane with fixed total energy are shown in Fig. 8. Only four examples are shown, and more examples will be listed in Fig. 11 in the Appendix. As numerical results as well as Fig. 11 reveal, oscillation only appears in the radial direction of the transverse plane, although the total final-momentum distribution has three dimensions. This can only be explained by the effect of smearing due to the two-dimensional integral in Eq. (7). We have seen that the distribution of the general monochromatic vortex collision has been partly smeared out by a one-dimensional integral. For the Laguerre-Gaussian case, a two-dimensional integral works more effectively. The oscillation of the final distribution in the longitudinal and energetic directions are completely smeared out, while oscillation in the transverse direction is just partly smeared out. A direct result of this change is that the topological charge-induced forward-backward asymmetry is difficult to see in the Laguerre-Gaussian case. The distributions also display topological structures in this case. According to pictures with different initial topological charges, we conclude that the topological charge dependence is

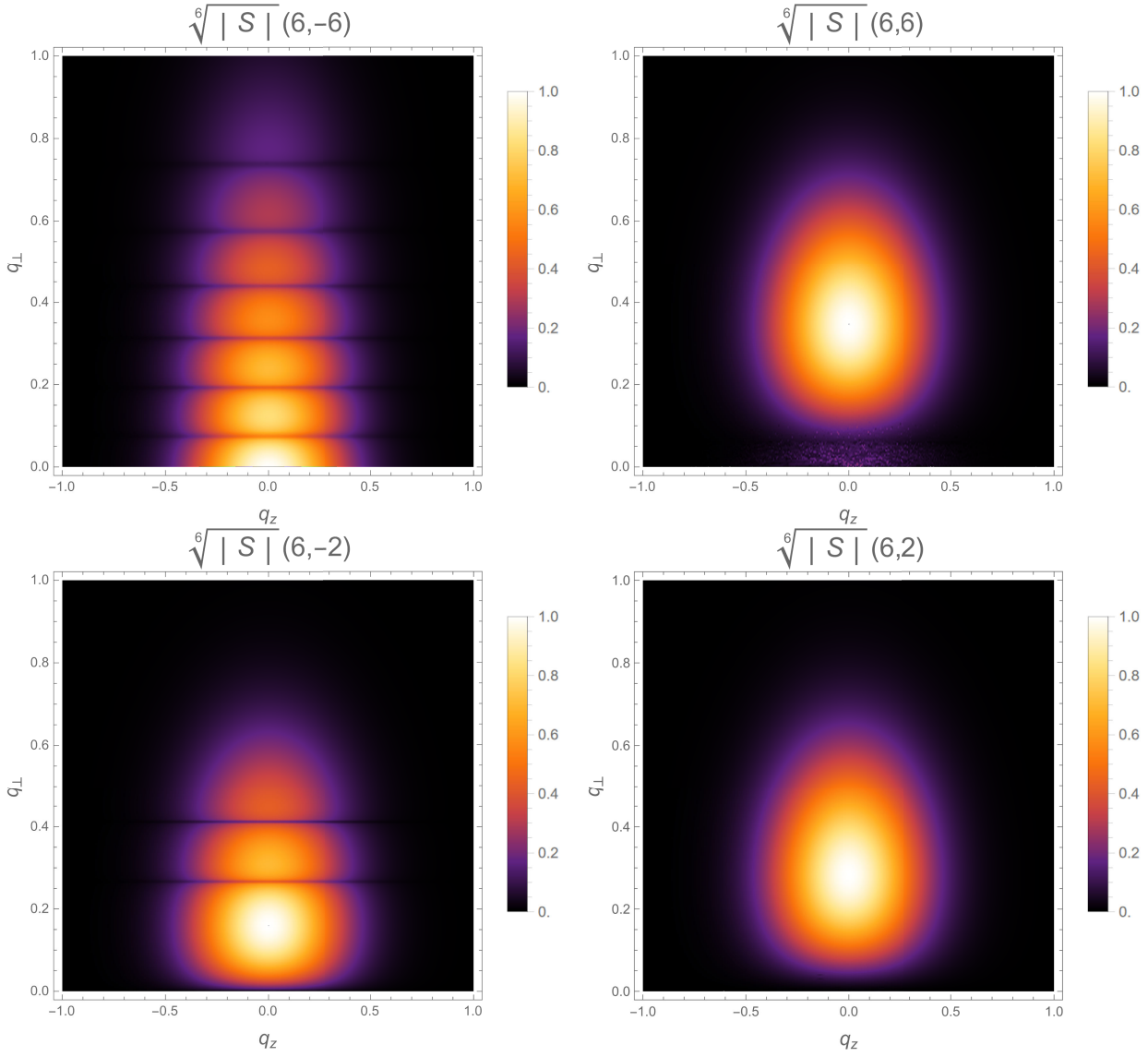

FIG. 8. Two-dimensional oscillation patterns of a $\sqrt[6]{|\mathcal{S}|}$ distribution at fixed total energy ($E_q = 4$ MeV) for a Laguerre-Gaussian vortex states collision. The distribution has been normalized so that its biggest value is 1. We set ($\ell_1 = -\ell_2 = 6$) for the top-left picture, ($\ell_1 = \ell_2 = 6$) for the top-right picture, ($\ell_1 = 6, \ell_2 = -2$) for the bottom-left picture, and ($\ell_1 = 6, \ell_2 = 2$) for the bottom-right picture. Other parameters of initial states: $\bar{k}_{z1} = \bar{k}_{z2} = 2$ MeV, $\sigma_{z1} = \sigma_{z2} = \sigma_{\perp 1} = \sigma_{\perp 2} = 0.1$ MeV, $n_1 = n_2 = 0$.

$$n^L = n_\perp^L + n_z^L - 1, \qquad n_\perp^L = \frac{|\ell_1| + |\ell_2| - |\ell_1 + \ell_2|}{2} + 1,$$
$$n_z^L = 1.$$

The superscript "L" represents the initial Laguerre-Gaussian vortex states. We can see that $n_\perp^L$ and $n_\perp^M$ have the same topological charge dependence. This is a nice result and means that it may be a general principle for physical vortex state collisions. Thus, it may be used for the measurement of a vortex state's topological charge.

Another obvious feature is that the distribution near the z axis tends to zero for almost all subpictures in Fig. 11 except for the case that satisfies $\ell_1 + \ell_2 \equiv 0$. We see that the distribution near the z axis is nonzero and relatively large for this special case. In fact, this effect can be calculated analytically by Eq. (7). Setting q_z (the longitudinal part of the total momentum $\mathbf{q}$) equal to zero, we find that

$$\mathcal{S}(L_1 + L_2 \to P_3 + P_4) \propto \int_0^\pi d\varphi_1 \cos[(\ell_1 + \ell_2)\varphi_1)]\mathcal{M}, \tag{8}$$

where another integral in Eq. (7) is not shown here because the two integrals are completely separated by setting

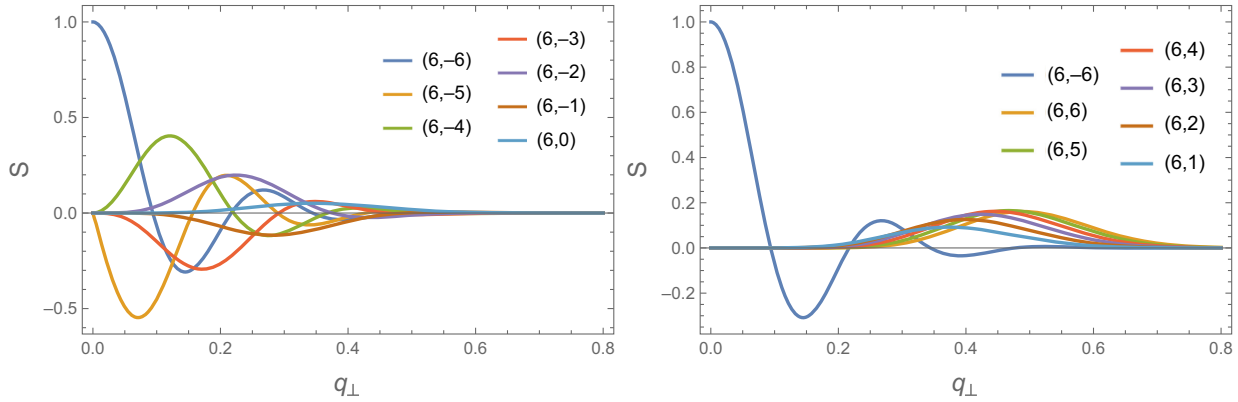

FIG. 9. One-dimensional $\mathcal{S}$ distributions at fixed total energy ($E_q = 4$ MeV) and total longitudinal momentum ($q_z = 0$ MeV) for a Laguerre-Gaussian vortex states collision. The distributions have been normalized so that the biggest value of the vertical coordinate is 1. Left: $\ell_1 = 6$ and $\ell_2 = -6, -5, -4, -3, -2, -1, 0$. Right: $\ell_1 = 6$ and $\ell_2 = -6, 1, 2, 3, 4, 5, 6$. Other parameters of initial states: $\bar{k}_{z1} = \bar{k}_{z2} = 2$ MeV, $\sigma_{z1} = \sigma_{z2} = \sigma_{\perp 1} = \sigma_{\perp 2} = 0.1$ MeV, $n_1 = n_2 = 0$.

$q_z = 0$. Equation (8) is nonzero only if $\ell_1 + \ell_2 = 0$. This feature characterizes the initial system of two vortex states with zero total angular momentum. It can also be used for the measurement of a vortex particle's topological charge. By the way, the oscillation of Laguerre-Gaussian vortex collision can also be shown by a one-dimensional transverse distribution, since longitudinal and energetic distributions are completely smeared out. Pictures of this kind are shown in Fig. 9. By these figures, the feature becomes much more clear.

IV. CONCLUSIONS AND THE OUTLOOK

In this work, using qualitative calculations and discussions, we investigated the peculiar topological features which arise in the final-momentum distributions in scalar vortex states collisions. We compared the results for three kinds of vortex states: the Bessel, a general monochromatic, and the Laguerre-Gaussian vortex states. The main findings are as follows:

(1) The total final-momentum distribution possesses a peculiar topological structure in momentum space in the following sense: The distribution is partitioned into several concentric doughnut-like regions by multiple $\mathcal{S} = 0$ surfaces. The number of these disjoint regions is fully determined by the topological charges of the initial states.

(2) The total final-momentum distributions show an additional feature which is characteristic for the case $\ell_1 + \ell_2 = 0$, which means that the angular momentum of the entire initial state is zero. Namely, only in this case can the distribution in the vicinity of the z axis be nonzero and relatively large. This is especially clear for the Laguerre-Gaussian vortex collision case. Note that most experimental vortex states are formulated as Laguerre-Gaussian states.

Both features provide methods to measure an unknown topological charge of a vortex particle (or beam) when it collides with a vortex target with a known topological charge. Whether they can be applied to realistic scattering of vortex states requires detailed quantitative computations. These calculations should be done with the Laguerre-Gaussian vortex particles, because they are readily generated in experiments.

Other properties of vortex particle collision discussed in this paper include a "smearing-out" effect, analogous to what is seen in two-slit interference and an unusual forward-backward asymmetry induced by $|\ell_1| \neq |\ell_2|$, which manifests itself only for the general monochromatic vortex particles. We hope that all these features will remain in realistic collisions of vortex electrons and other particles.

ACKNOWLEDGMENTS

We thank Professor Igor P. Ivanov in the School of Physics and Astronomy in Sun Yat-sen University for instructive suggestions and helpful discussions. This work was supported by the Fundamental Research Funds for the Central Universities at Sun Yat-sen University.

APPENDIX: DEPENDENCE OF THE MOMENTUM-SPACE DISTRIBUTIONS ON ℓ

Here, for completeness, we show how the momentum-space distributions for the monochromatic and Laguerre-Gaussian states depend on the values of the topological charge ℓ_2 with a fixed ℓ_1.

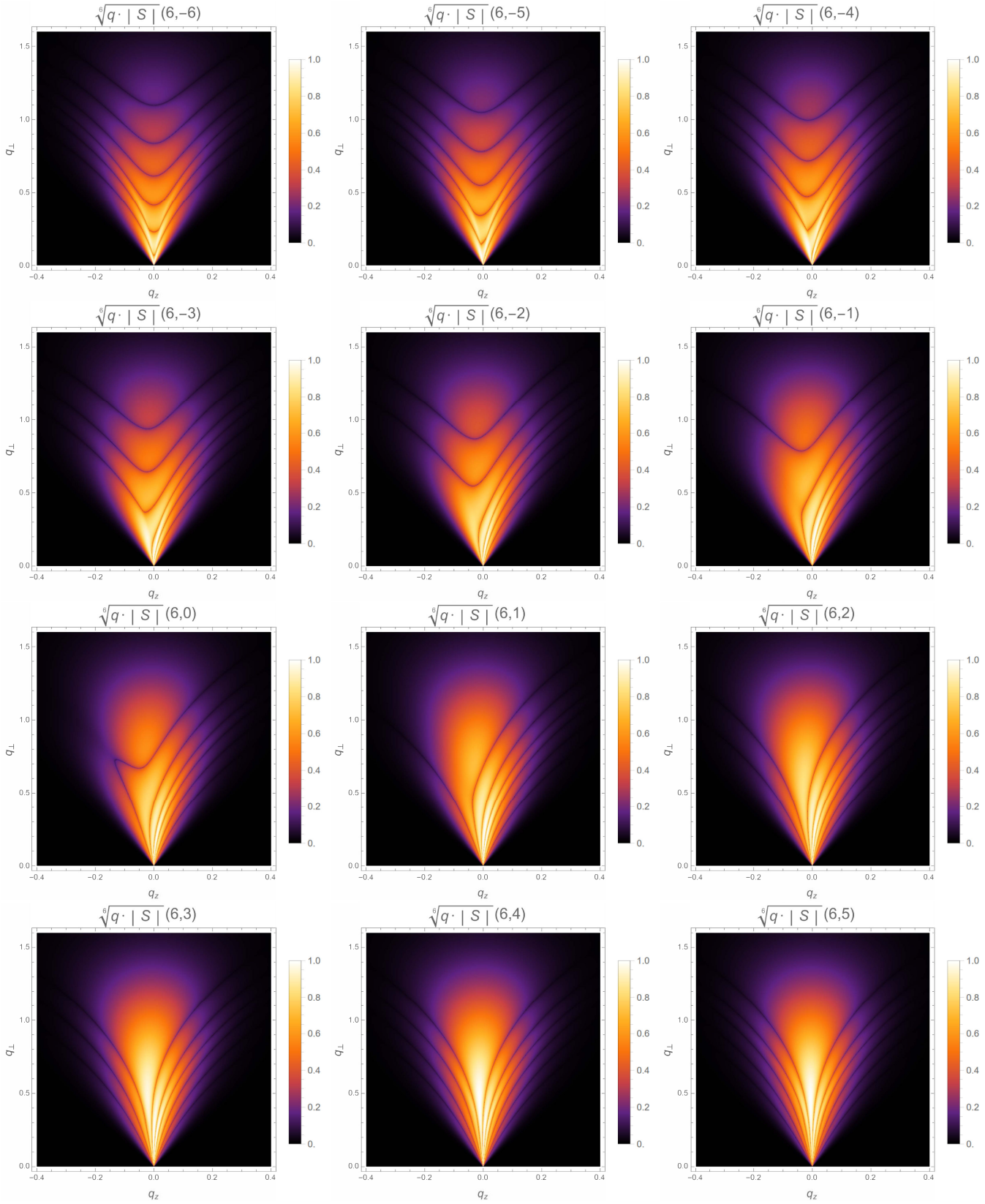

FIG. 10. Two-dimensional oscillation patterns of $\sqrt[6]{|\mathcal{S}|}$ distribution for general monochromatic vortex states collision. The distribution has been normalized so that its biggest value is 1. (ℓ_1, ℓ_2) is shown in every subpicture. Other parameters of initial states: $E_1 = E_2 = 2$ MeV, $\theta_{01} = \theta_{02} = \sigma_{01} = \sigma_{02} = 0.1$ rad.

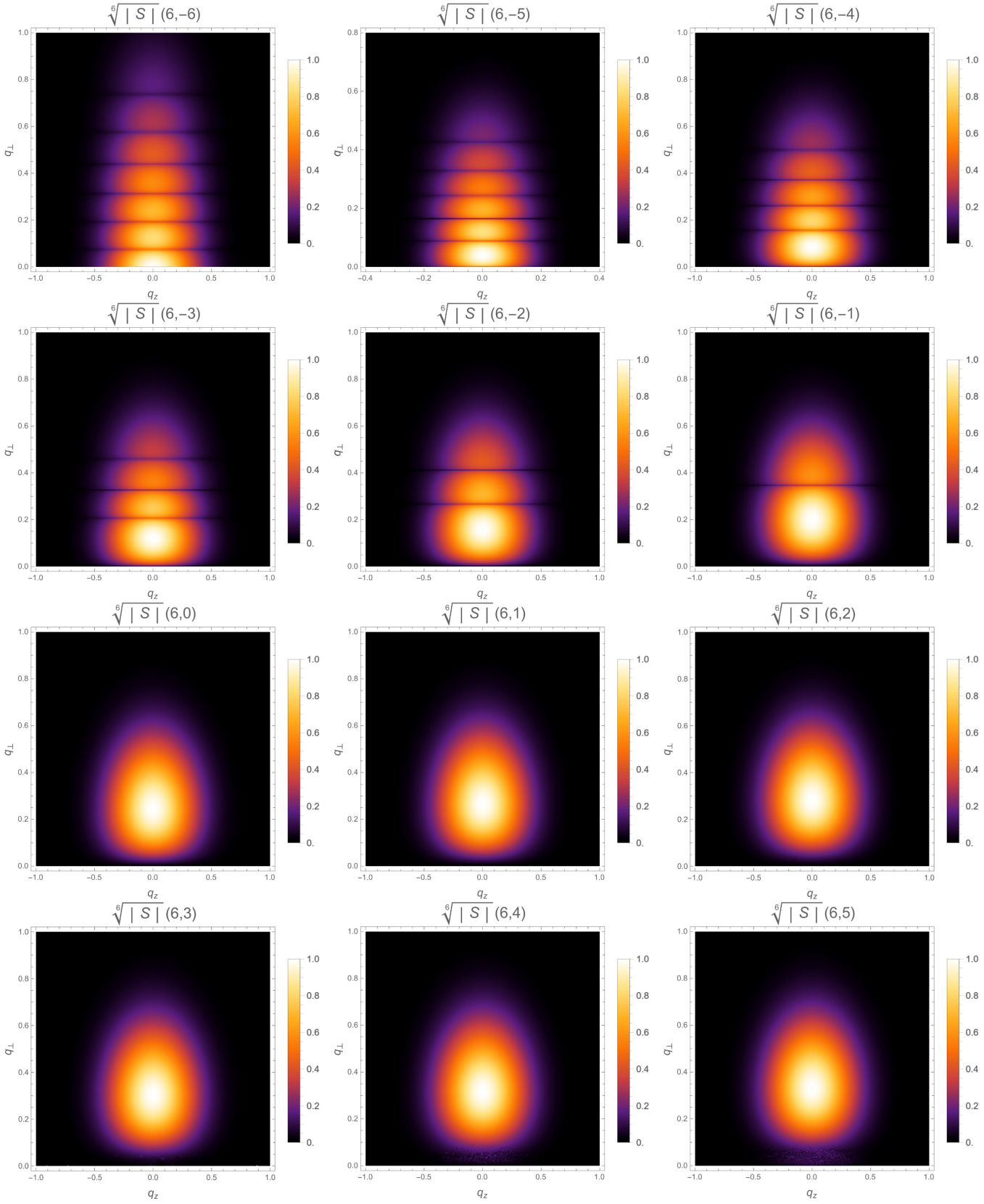

FIG. 11. Two-dimensional oscillation patterns of $\sqrt[6]{|\mathcal{S}|}$ distributions at fixed total energy ($E_q = 4$ MeV) for a Laguerre-Gaussian vortex states collision. The distribution has been normalized so that its biggest value is 1. (ℓ_1, ℓ_2) is shown in every subpicture. Other parameters of initial states: $\bar{k}_{z1} = \bar{k}_{z2} = 2$ MeV, $\sigma_{z1} = \sigma_{z2} = \sigma_{\perp 1} = \sigma_{\perp 2} = 0.1$ MeV, $n_1 = n_2 = 0$.

[1] A. E. Blinov, A. E. Bondar, Y. I. Eidelman *et al.*, Phys. Lett. **113B**, 423 (1982).
[2] V. N. Baier and V. M. Katkov, Phys. Rev. D **66**, 053009 (2002).
[3] K. Melnikov, G. L. Kotkin, and V. G. Serbo, Phys. Rev. D **54**, 3289 (1996).
[4] K. Melnikov and V. G. Serbo, Nucl. Phys. **B483**, 67 (1997).
[5] D. V. Karlovets, G. L. Kotkin, and V. G. Serbo, Phys. Rev. A **92**, 052703 (2015).
[6] L. Sarkadi, I. Fabre, F. Navarrete, and R. O. Barrachina, Phys. Rev. A **93**, 032702 (2016).
[7] K. Y. Bliokh, I. P. Ivanov, G. Guzzinati *et al.*, Phys. Rep. **690**, 1 (2017).
[8] I. P. Ivanov, Prog. Part. Nucl. Phys. **127**, 103987 (2022).
[9] M. W. Beijersbergen, R. P. C. Coerwinkel, and J. P. Woerdman, Opt. Commun. **112**, 321 (1994).
[10] M. Uchida and A. Tonomura, Nature (London) **464**, 737 (2010).
[11] C. W. Clark, R. Barankov, M. G. Huber, M. Arif, D. G. Cory, and D. A. Pushin, Nature (London) **525**, 504 (2015).
[12] A. Luski, Y. Segev, R. David, O. Bitton, H. Nadler, A. Ronny Barnea, A. Gorlach, O. Cheshnovsky, I. Kaminer, and E. Narevicius, Science **373**, 1105 (2021).
[13] N. B. Simpson, K. Dholakia, L. Allen, and M. J. Padgett, Opt. Lett. **22**, 52 (1997).
[14] J. E. Curtis, B. A. Koss, and D. G. Grier, Opt. Commun. **207**, 169 (2002).
[15] K. Ladavac and D. G. Grier, Opt. Express **12**, 1144 (2004).
[16] J. Leach, B. Jack, J. Romero, A. K. Jha, A. M. Yao, S. Franke-Arnold, D. G. Ireland, R. W. Boyd, S. M. Barnett, and M. J. Padgett, Science **329**, 662 (2010).
[17] J. Wang, J. Y. Yang, I. M. Fazal *et al.*, Nat. Photonics **6**, 488 (2012).
[18] J. Yuan, S. M. Lloyd, and M. Babiker, Phys. Rev. A **88**, 031801(R) (2013).
[19] A. Konecna, M. K. Schmidt, R. Hillenbrand, and J. Aizpurua, Phys. Rev. Res. **5**, 023192 (2023).
[20] R. Juchtmans and J. Verbeeck, Phys. Rev. A **93**, 023811 (2016).
[21] L. Zou, P. Zhang, and A. J. Silenko, J. Phys. B **57**, 045401 (2024).
[22] S. S. Baturin, D. V. Grosman, G. K. Sizykh, and D. V. Karlovets, Phys. Rev. A **106**, 042211 (2022).
[23] G. K. Sizykh, A. D. Chaikovskaia, D. V. Grosman, I. I. Pavlov, and D. V. Karlovets, Phys. Rev. A **109**, L040201 (2024).
[24] V. K. Ivanov, A. D. Chaikovskaia, and D. V. Karlovets, Phys. Rev. A **108**, 062803 (2023).
[25] V. Serbo, I. P. Ivanov, S. Fritzsche, D. Seipt, and A. Surzhykov, Phys. Rev. A **92**, 012705 (2015).
[26] I. P. Ivanov, B. Liu, and P. M. Zhang, Phys. Rev. A **105**, 013522 (2022).
[27] Pengcheng Zhao, I. P. Ivanov, and Pengming Zhang, Phys. Rev. D **104**, 036003 (2021).
[28] P. C. Zhao, J. Phys. G **50**, 15 (2023).
[29] A. Afanasev, C. E. Carlson, and A. Mukherjee, Phys. Rev. Res. **3**, 023097 (2021).
[30] A. Afanasev and C. E. Carlson, Ann. Phys. (Berlin) **534**, 9 (2022).
[31] Bei Liu and I. P. Ivanov, Phys. Rev. A **107**, 063110 (2023).
[32] I. P. Ivanov, Phys. Rev. D **83**, 093001 (2011).
[33] I. P. Ivanov, Phys. Rev. D **85**, 076001 (2012).
[34] I. P. Ivanov, D. Seipt, A. Surzhykov, and S. Fritzsche, Phys. Rev. D **94**, 076001 (2016).
[35] M. Hillery, L. Mlodinow, and V. Buzek, Phys. Rev. A **71**, 062103 (2005).